Taylor & Francis
Taylor & Francis Group

RESEARCH ARTICLE

Check for updates

Deacetylation of ATG7 drives the induction of macroautophagy and LC3-associated microautophagy

Yinfeng Xu[a], Chuying Qian[b], Qian Wang[b], Lijiang Song[b], Zhengfu He[b], Wei Liu[c], and Wei Wan [b]

[a]Laboratory of Basic Biology, Hunan First Normal University, Changsha, Hunan, China; [b]Department of Biochemistry, and Department of Thoracic Surgery of Sir Run Run Shaw Hospital, Zhejiang University School of Medicine, Hangzhou, Zhejiang, China; [c]Department of Metabolic Medicine, International Institutes of Medicine, the Fourth Affiliated Hospital, Zhejiang University School of Medicine, Yiwu, Zhejiang, China

ABSTRACT

LC3 lipidation plays an important role in the regulation of macroautophagy and LC3-associated micro-autophagy. The E1-like enzyme ATG7 is one of the core components that are directly involved in LC3 lipidation reaction. Here, we provide evidence showing that acetylation of ATG7 tightly controls its enzyme activity to regulate the induction of macroautophagy and LC3-associated microautophagy. Mechanistically, acetylation of ATG7 disrupts its interaction with the E2-like enzyme ATG3, leading to an inhibition of LC3 lipidation *in vitro* and *in vivo*. Functionally, in response to various different stimuli, cellular ATG7 undergoes deacetylation to induce macroautophagy and LC3-associated microautophagy, which are necessary for cells to eliminate cytoplasmic DNA and degrade lysosome membrane proteins, respectively. Taken together, these findings reveal that ATG7 acetylation acts as a critical rheostat in controlling LC3 lipidation and related cellular processes.

Abbreviations: AMPK: AMP-activated protein kinase; ATG: autophagy-related; cGAMP: cyclic GMP-AMP; CGAS: cyclic GMP-AMP synthase; CREBBP/CBP: CREB binding protein; EGF: epidermal growth factor; EGFR: epidermal growth factor receptor; EP300/p300: E1A binding protein p300; IFNB1: interferon beta 1; ISD: interferon stimulatory DNA; MAP1LC3/LC3: microtubule associated protein 1 light chain 3; MCOLN1/TRPML1: mucolipin TRP cation channel 1; MEF: mouse embryonic fibroblast; MTOR: mechanistic target of rapamycin kinase; NAM: nicotinamide; PE: phosphatidylethanolamine; PTM: post-translational modification; RB1CC1/FIP200: RB1 inducible coiled-coil 1; SIRT: sirtuin; SQSTM1/p62: sequestosome 1; STING1: stimulator of interferon response cGAMP interactor 1; TSA: trichostatin A; ULK1: unc-51 like autophagy activating kinase 1; WIPI2: WD repeat domain, phosphoinositide interacting 2; WT: wild-type.

Introduction

Autophagy is a highly conserved lysosome-dependent degradation process in eukaryotic cells [1,2]. According to cargo delivery to the lysosome, autophagy is mainly classified into three types: macroautophagy, microautophagy and chaperone-mediated autophagy [3,4]. Macroautophagy is featured with the formation of double-membrane autophagosomes, which sequester the substrates and fuse with lysosomes [5]. During microautophagy, lysosomes directly engulf the substrates through the invagination or protrusion of the lysosomal membrane [6]. For chaperone-mediated autophagy, the proteins containing KFERQ-like motifs are recognized by chaperones and transported into lysosomes across the channels formed with LAMP2A (lysosomal associated membrane protein 2A) oligomers on lysosomal membrane [7]. Accumulating evidence has demonstrated that autophagy is essential for the maintenance of cellular homeostasis by controlling the degradation of various intracellular materials, such as unwanted proteins, damaged organelles and invading pathogens. Dysfunction of autophagy is highly linked to the pathogenesis of a wide array of human diseases, including several types of cancers and neurodegenerative diseases [8–10].

The lipidation of MAP1LC3/LC3 (microtubule associated protein 1 light chain 3) and other Atg8 (autophagy-related 8)-family proteins is a key event in macroautophagy (we use LC3 hereafter to refer to all Atg8-family proteins for simplicity). Lipidated LC3 is involved in the regulation of multiple steps, including autophagy induction, autophagosome formation, cargo recruitment and autophagosome-lysosome fusion [11–15]. Recently, several studies have reported that lipidated LC3 also plays a pivotal role in microautophagy by controlling the selectivity and recruitment of the substrates [16,17]. Of note, LC3 lipidation reaction converts soluble LC3 into membrane-bound form, permitting LC3 to function in both macroautophagy and LC3-associated microautophagy [11–17]. The lipidation of LC3 in the cell requires a number of components to function in a sequential manner. At first, full-length LC3 is cleaved by protease ATG4 to expose the C-terminal G120. Then, the lipid phosphatidylethanolamine (PE) is conjugated with LC3 at G120 to form membrane-bound LC3–PE under the assistance of two ubiquitin-like enzymatic cascades. Notably, the final cognate reaction for LC3–PE formation is orchestrated by the E1-like enzyme ATG7, the E2-like enzyme

ATG3 and the E3-like enzyme ATG12–ATG5-ATG16L1 complex [18].

Protein acetylation has emerged as a master regulator for LC3 lipidation [1]. Several components, among the core machinery for LC3 lipidation, are regulated by protein acetylation [19–23]. Acetylation of ATG3 promotes its binding to LC3 and leads to the activation of LC3 lipidation [19]. Intriguingly, acetylation of ATG4 and LC3 seems to play an inhibitory role [20,23]. Acetylation of ATG4 suppresses the cleavage of full-length LC3 by decreasing its affinity for LC3, and acetylation of nuclear LC3 blocks its cytoplasmic translocation and subsequent binding to ATG7 [20,23]. Both of these two mechanisms are utilized by the cell to inhibit LC3 lipidation under nutrient-rich conditions [20,23]. However, the regulatory role of acetylation of other core components, including ATG5, ATG7 and ATG12, in LC3 lipidation reaction remains elusive. Considering that LC3 lipidation is involved in the regulation of both macroautophagy and LC3-associated microautophagy [16,17,24], it would be worthwhile investigating the function and mechanism of acetylation of these autophagy-related proteins in LC3 lipidation and related cellular processes.

In this study, we report that cellular ATG7 undergoes deacetylation in response to many different stimuli. We demonstrate that deacetylation of ATG7 enhances its affinity for ATG3 and promotes LC3 lipidation *in vitro* and *in vivo*. Functionally, we show that deacetylation of ATG7 is required for the initiation of canonical and non-canonical macroautophagy, and the latter is responsible for the clearance of cytoplasmic DNA. In addition, we reveal that deacetylation of ATG7 drives the induction of LC3-associated microautophagy, which promotes the selective turnover of lysosome membrane proteins to maintain lysosome activity.

Results

Identification of the acetylation sites of ATG7

We began by checking the acetylation of ATG7 in cells. The cells were treated with nicotinamide (NAM), an inhibitor of SIRT (sirtuin) family deacetylases, or trichostatin A (TSA), an inhibitor of HDAC family deacetylases, and we found that only NAM treatment significantly elevated the acetylation level of ATG7 (Figure 1A,B). In addition, we treated the cells with C646, an inhibitor of acetyltransferases EP300/p300 (E1A binding protein p300) and CREBBP/CBP (CREB binding protein), or EX-527, an inhibitor of deacetylase SIRT1, and found that the acetylation level of ATG7 was decreased and increased, respectively (Figure 1C,D). Consistent results were also obtained in cells with knockdown of *EP300-CREBBP* or *SIRT1* (Figure 1E,F). These results confirm the previous observations that ATG7 acetylation is coordinately controlled by EP300-CREBBP and SIRT1 [21,22]. We then performed *in vitro* acetylation assays using purified EP300-Flag and recombinant GST-ATG7. Obviously, wild-type (WT) EP300, but not inactive EP300 mutant (S1396R, Y1397R) [25], acetylated ATG7 in the presence of acetyl-CoA (Figure 1G). Consistent with this, C646 treatment failed EP300 to acetylate ATG7 (Figure 1G). These data suggest that ATG7 can be directly acetylated by EP300. To identify

the acetylation site(s) of ATG7, acetylated ATG7 from the *in vitro* acetylation assay was subjected to mass spectrometry analysis. K284 and K296, which are conserved across species, were suggested (Figure 1H and S1). We then generated an ATG7 mutant by replacing all the two lysine residues with arginine residues, and performed *in vitro* acetylation assays using purified EP300-Flag and recombinant GST-tagged ATG7 or ATG7-2KR (K284R,K296R), mimicking the acetylation-disabled ATG7. As expected, WT ATG7 but not ATG7-2KR was markedly acetylated by EP300 (Figure 1I,J).
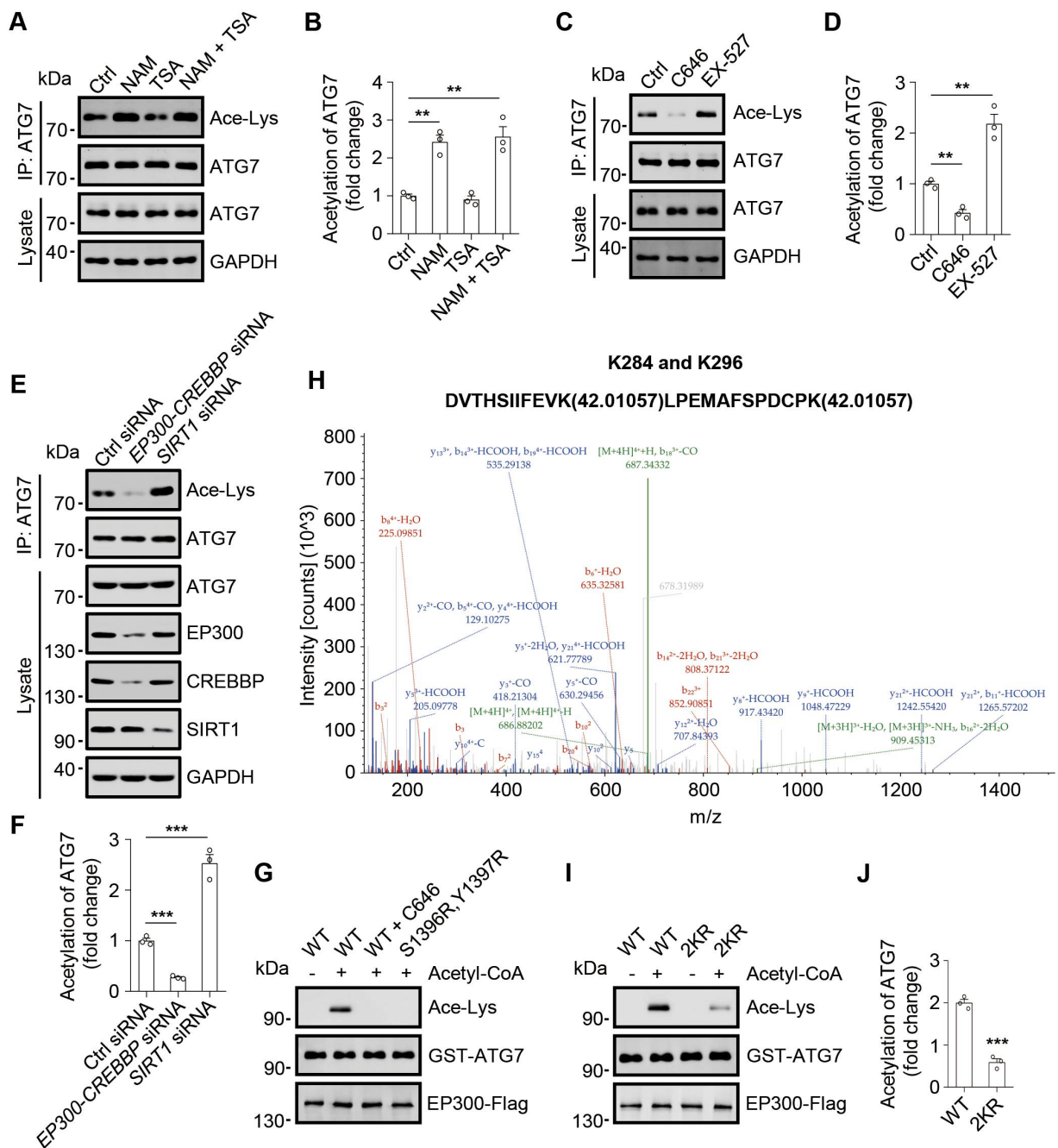
Acetylation of ATG7 inhibits LC3 lipidation

As nutrient deprivation and mechanistic target of rapamycin kinase (MTOR) complex 1 (MTORC1) inhibitor treatment are two widely used inducers for LC3 lipdation, we checked whether the acetylation of ATG7 in cells is regulated by these stimuli. Treatment of the cells with starvation medium or torin1, an inhibitor of MTORC1, significantly decreased the acetylation level of ATG7 (Figure 2A,B). Moreover, incubation of the starved or torin1-treated cells with fresh culture medium reversed the decrease of the acetylation of ATG7 (Figure 2A,B). We also examined the effect of re-stimulation of nutrients on the acetylation of WT ATG7 and ATG7 mutants. Compared with WT ATG7, ATG7^{K284R} and ATG7^{K296R} displayed lower acetylation levels, and ATG7-2KR exhibited the lowest acetylation level (Figure 2C,D). These results suggest that the acetylation of ATG7 in the cell is regulated by nutrient status, and K284 and K296 are the two major responding acetylation sites.

To test whether acetylation of ATG7 influences its E1-like enzyme activity, we performed *in vitro* LC3 lipidation assays using cytosol from *atg7* knockout cells and membranes from *atg5* knockout cells (Figure 2E) [26]. Obviously, WT ATG7 from cells treated with CTB, an activator of EP300-CREBBP, or ATG7^{C567S}, an inactive mutant [27], from cells treated with normal culture medium, significantly inhibited LC3 conversion (Figure 2F,G). Furthermore, ATG7-2KQ, but not WT ATG7 or ATG7-2KR, failed to stimulate LC3–PE production (Figure 2H, I). These data suggest that acetylation of ATG7 inhibits LC3 lipidation by decreasing its E1-like enzyme activity.

Acetylation of ATG7 inhibits its binding to ATG3

ATG7 needs to interact with LC3 and ATG3 to exert its E1-like enzyme activity [28–30]. To investigate the underlying mechanism by which acetylation of ATG7 inhibits LC3 lipidation, we began by checking the interaction between LC3 and ATG7. Consistent with a previous study [20], LC3-2KQ (K49Q,K51Q) failed to pull down ATG7 (Figure 3A,B). However, compared with WT ATG7, WT LC3 pulled down similar amounts of ATG7-2KR or ATG7-2KQ (Figure 3A,B). We then examined whether acetylation of ATG7 regulates its binding to ATG3. Compared with WT ATG7 or ATG7-2KR, ATG7-2KQ pulled down lower amounts of ATG3 (Figure 3C,D). In addition, we performed *in vitro* acetylation assays using WT ATG7 and ATG7 mutants, and then checked their interactions with ATG3. The results showed that incubation with acetyl-CoA only reduced the interaction between WT ATG7 and ATG3 (Figure 3E,F). We also

Figure 1. Identification of the acetylation sites of ATG7. (A) acetylation of ATG7 in HEK293 cells treated with or without nicotinamide (NAM), an inhibitor of SIRT family deacetylases, and/or trichostatin a (TSA), an inhibitor of HDAC family deacetylases. ATG7 was immunoprecipitated from the cell lysate with an anti-ATG7 antibody, and the immunoprecipitates were analyzed by western blot using an anti-acetyl-lysine antibody (Ace-Lys). (B) statistical analysis of (A). (C) acetylation of ATG7 in HEK293 cells treated with or without C646, an inhibitor of acetyltransferases EP300-CREBBP, or EX-527, an inhibitor of deacetylase SIRT1. (D) statistical analysis of (C). (E) acetylation of ATG7 in HEK293 cells treated with either nontargeting siRNA or siRNAs for *EP300-CREBBP* or *SIRT1*. (F) statistical analysis of (E). (G) *in vitro* acetylation assays of ATG7. Purified recombinant GST-ATG7 from *Escherichia coli* BL21 cells was incubated with immunoprecipitated Flag-tagged wild-type (WT) EP300 or EP300^{S1396R,Y1397R}, an inactive mutant, from 293T cells, with or without acetyl-CoA and C646. (H) MS/MS spectrum of the tryptic peptide (inset) from recombinant ATG7 protein underwent *in vitro* acetylation assay with a mass shift of 42.01057 Da at the lysine residue. (I) *in vitro* acetylation assays of WT ATG7 or ATG7-2KR (K284R,K296R) with or without acetyl-CoA in the presence of EP300-Flag. (J) statistical analysis of (I). All statistical data are presented as mean ± SEM of three independent experiments. **$p < 0.01$, ***$p < 0.001$ (Student's *t*-test).

examined the interaction between ATG7 and ATG3 in cells. As expected, ATG7-ATG3 interaction was increased and decreased when the cells were treated with C646 and EX-527, respectively (Figure 3G,H). Consistent with this, ATG3 binding to ATG7 was increased in cells expressing ATG7-2KR but decreased in cells expressing ATG7-2KQ (Figure 3I,J). Moreover, torin1 treatment only enhanced the interaction between WT ATG7 and ATG3

(Figure 3I,J). Taken together, these data suggest that acetylation of ATG7 inhibits its binding to ATG3 but not LC3.

Deacetylation of ATG7 is essential for macroautophagy

Given that LC3 lipidation is involved in the regulation of several distinct steps of macroautophagy, such as
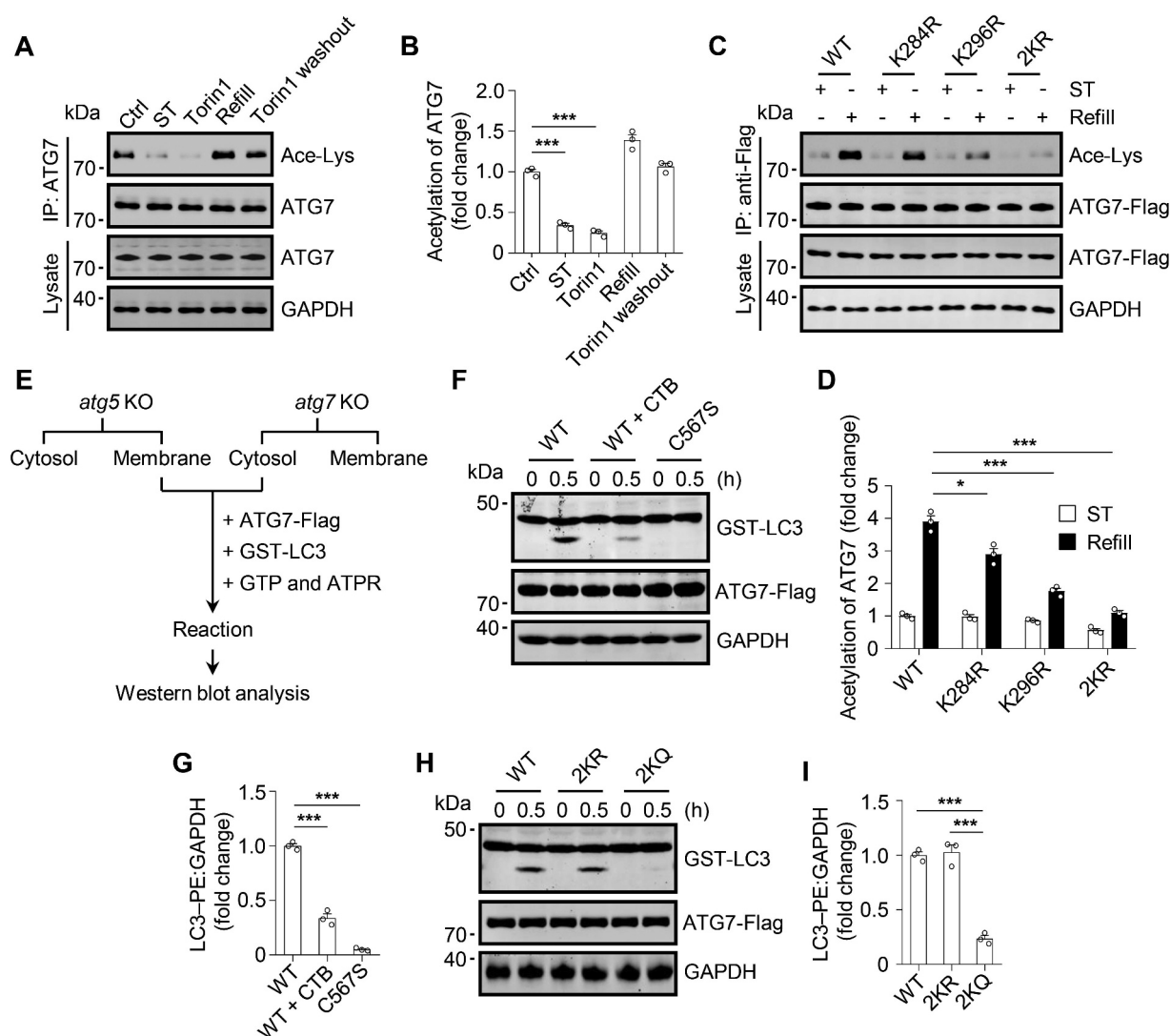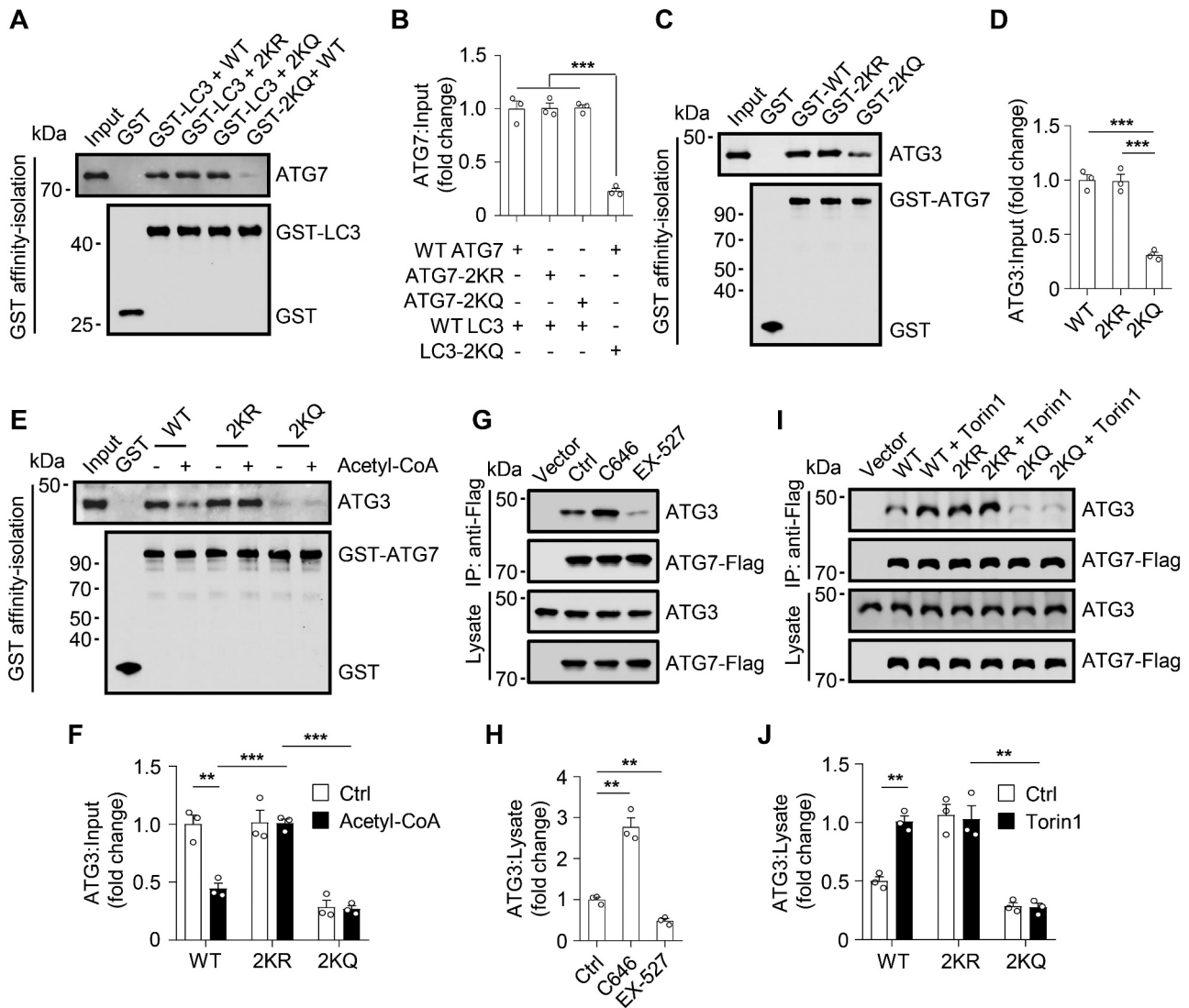
Figure 2. Acetylation of ATG7 inhibits LC3 lipidation. (A) acetylation of ATG7 in HEK293 cells. The cells were treated with starvation medium (ST) or torin1, an inhibitor of MTORC1, or followed by fresh culture medium treatment. (B) statistical analysis of (A). (C) acetylation of Flag-tagged WT ATG7 or ATG7 mutants in HEK293 cells. The cells were starved or re-stimulated with fresh culture medium. (D) statistical analysis of (C). (E) schematic of the workflow for in vitro reconstitution of LC3 lipidation. Purified GST-LC3 (LC3-G120, the processed form of LC3) and Flag-tagged WT ATG7 or ATG7 mutants were incubated with the membranes from atg5 knockout mouse embryonic fibroblasts (MEFs) and the cytosol from atg7 knockout MEFs plus GTP and an ATP regeneration system (ATPR) for the indicated times. Then the reaction was terminated and the generated LC3–PE was subjected to western blot analysis. (F) the in vitro LC3 lipidation assays were carried out using Flag-tagged WT ATG7 or ATG7^C567S, an inactive mutant, from 293T cells treated with or without CTB, an EP300-CREBBP activator. (G) statistical analysis of LC3–PE production in (F). (H) the in vitro LC3 lipidation assays were carried out using Flag-tagged WT ATG7, ATG7-2KR or ATG7-2KQ from 293T cells. (I) statistical analysis of LC3–PE production in (H). All statistical data are presented as mean ± SEM of three independent experiments. *$p < 0.05$, ***$p < 0.001$ (Student's t-test).

autophagosome formation [11,13,20], we first checked the role of ATG7 acetylation in autophagosome formation. As expected, knockout of atg7 abolished GFP-LC3 punctum formation in torin1-treated cells (Fig. S2A,B). We then re-introduced WT ATG7, ATG7-2KR or ATG7-2KQ into atg7 knockout cells and generated stable cell lines (Fig. S2C). Interestingly, re-introduction of WT ATG7 or ATG7-2KR but not ATG7-2KQ restored GFP-LC3 punctum formation in starved cells (Figure 4A,B). Consistent with this, knockout of atg7 from the cell resulted in a significant accumulation of SQSTM1/p62 (sequestosome 1), one of autophagy receptor proteins (Figure 4C,D). Re-introduction of WT ATG7 or ATG7-2KR but not ATG7-2KQ into atg7 knockout cells abolished the increase of SQSTM1 protein level (Figure 4C,D). Moreover, torin1 treatment markedly stimulated LC3–PE

formation and SQSTM1 degradation in atg7 knockout cells with re-introduction of WT ATG7 or ATG7-2KR but not ATG7-2KQ (Figure 4C–E). These results suggest that deacetylation of ATG7 is required for autophagosome formation and autophagic degradation during nutrient-sensing pathway-regulated macroautophagy.

In addition to nutrient-regulated canonical macroautophagy, LC3 lipidation is recently shown to be required for STING1 (stimulator of interferon response cGAMP interactor 1)-induced non-canonical macroautophagy [31–34]. We began by checking ATG7 acetylation, and found that transfection of HT-DNA, activating CGAS (cyclic GMP-AMP synthase)-STING1 pathway, or treatment with cyclic GMP-AMP (cGAMP), activating STING1, significantly decreased the acetylation of ATG7 in cells (Fig. S3A,B). Furthermore,

Figure 3. Acetylation of ATG7 inhibits its binding to ATG3. (A) interaction between LC3 and ATG7. GST-tagged WT LC3 or LC3-2KQ (K49Q,K51Q) was incubated with WT ATG7, ATG7-2KR or ATG7-2KQ, and GST-tagged WT LC3 or LC3-2KQ was then pulled down using glutathione sepharose beads, and the bound ATG7 was analyzed by western blot. (B) statistical analysis of (A). (C) interaction between ATG7 and ATG3. GST-tagged WT ATG7, ATG7-2KR or ATG7-2KQ was incubated with ATG3 and the GST affinity-isolation assays were carried out using glutathione sepharose beads. (D) statistical analysis of (C). (E) interaction between ATG7 and ATG3. GST-tagged WT ATG7, ATG7-2KR or ATG7-2KQ was incubated with or without acetyl-CoA in the presence of EP300-Flag, and further incubated with ATG3 and followed by GST affinity-isolation assays. (F) statistical analysis of (E). (G) co-immunoprecipitation of Flag-tagged WT ATG7 with ATG3 in 293T cells treated with C646, an inhibitor of acetyltransferases EP300-CREBBP, or EX-527, an inhibitor of deacetylase SIRT1. The cells were lysed and incubated with anti-Flag magnetic beads, and the immunoprecipitates were subjected to western blot analysis using anti-ATG3. (H) statistical analysis of (G). (I) co-immunoprecipitation of Flag-tagged WT ATG7, ATG7-2KR or ATG7-2KQ with ATG3 in 293T cells treated with or without torin1. (J) statistical analysis of (I). All statistical data are presented as mean ± SEM of three independent experiments. **$p < 0.01$, ***$p < 0.001$ (Student's t-test).

cGAMP treatment stimulated LC3 lipidation in *atg7* knockout cells with re-introduction of WT ATG7 or ATG7-2KR but not ATG7-2KQ (Figure 4F,G). Consistent with this, ATG7-2KQ showed lower affinity for ATG3 and the affinity cannot be enhanced by cGAMP treatment (Fig. S3C,D). We also checked LC3–PE production in cells with knockout of *rb1cc1* (RB1 inducible coiled-coil 1), a necessary subunit of ULK1 (unc-51 like autophagy activating kinase 1) complex, and found that treatment of the cells with cGAMP but not torin1 stimulated LC3–PE formation (Fig. S3E), confirming that CGAS-STING1 pathway-induced LC3 lipidation is independent of ULK1 complex [31]. Moreover, the production of LC3–PE in these cGAMP-treated cells was abolished by *Atg7* knockdown, and that was restored by re-introduction of WT

ATG7 or ATG7-2KR but not ATG7-2KQ. (Fig. S3E). These data suggest that deacetylation of ATG7 is required for STING1-induced LC3 lipidation.

Finally, we chose to investigate the physiological significance of ATG7 acetylation by examining the clearance of cytoplasmic DNA, which can activate CGAS-STING1 pathway and undergo degradation through STING1-induced non-canonical macroautophagy [31,34]. Considering that STING1-induced LC3 lipidation can occur on both single-membrane vesicles and double-membrane autophagosomes [31,34,35], we checked whether cytoplasmic DNA can be engulfed by autophagosomes. Firstly, in cells transfected with Cy3 labeled-interferon stimulatory DNA (ISD), we found that both WIPI2 (WD repeat domain, phosphoinositide
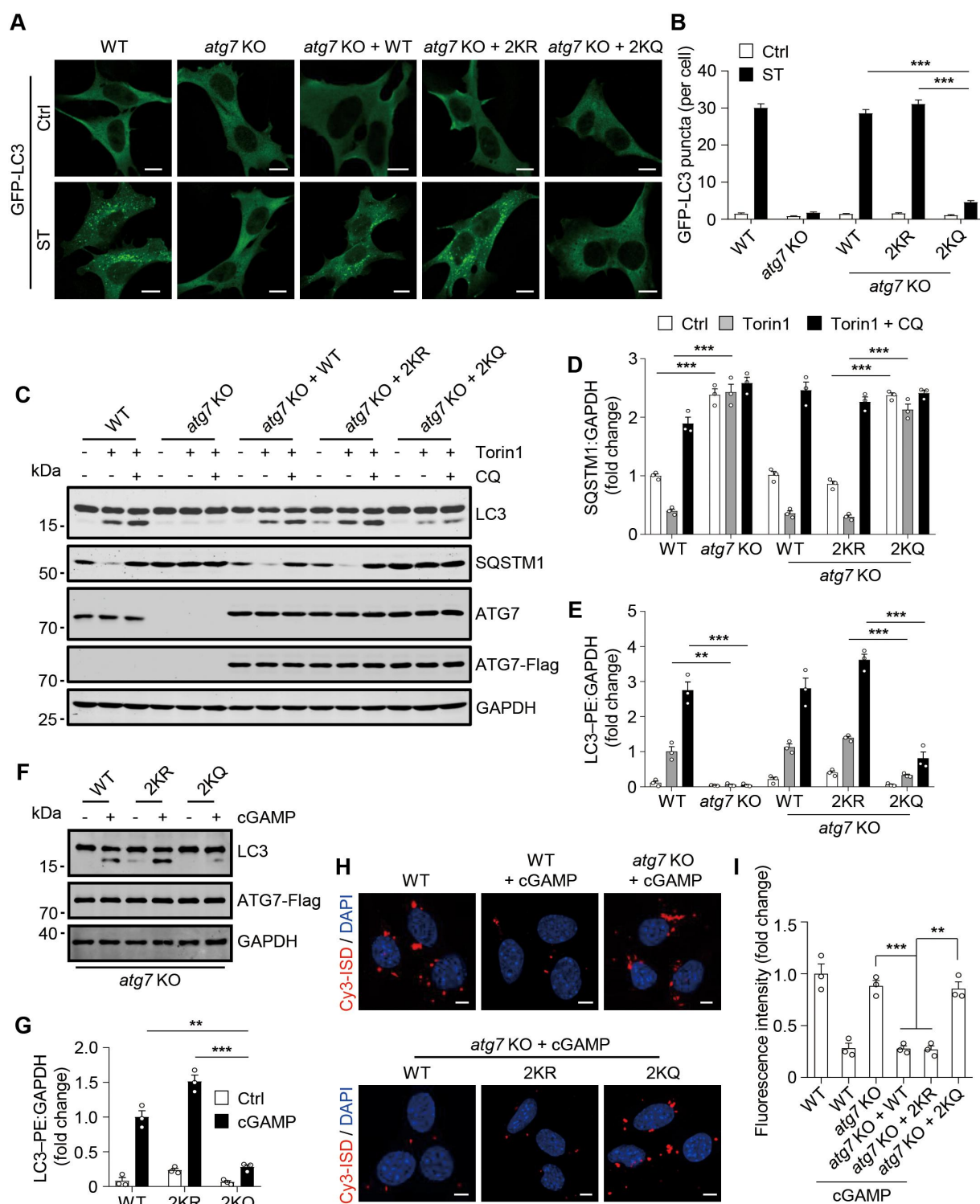
Figure 4. Deacetylation of ATG7 is essential for macroautophagy. (A) formation of GFP-LC3 puncta in MEFs stably expressing GFP-LC3. The cells with or without *atg7* knockout were re-introduced with WT ATG7, ATG7-2KR or ATG7-2KQ and treated with or without starvation medium (ST) for 1 h. (B) statistical analysis of the number of GFP-LC3 puncta in cells treated as in (A). $n = 30$. (C) the production of LC3–PE and the degradation of SQSTM1 in MEFs treated with or without torin1 or chloroquine (CQ) for 3 h. The cells with or without *atg7* knockout were re-introduced with WT ATG7, ATG7-2KR or ATG7-2KQ. (D and E) statistical analysis of the protein levels of SQSTM1 and LC3–PE in (C). (F) LC3 conversion in *atg7* knockout MEFs with re-introduction of WT ATG7, ATG7-2KR or ATG7-2KQ. The cells were treated with or without cGAMP. (G) statistical analysis of LC3–PE production in (F). (H) the clearance of cytoplasmic DNA in WT or *atg7* knockout MEFs re-introduced with WT ATG7, ATG7-2KR or ATG7-2KQ. The cells were transfected with Cy3 labeled-ISD (Cy3-ISD) (4 μg/ml) for 6 h and then stimulated by cGAMP for another 12 h. (I) statistical analysis of the fluorescence intensity of Cy3-ISD in cells treated as in (H). All the statistical data are presented as mean ± SEM of three independent experiments. **$p < 0.01$, ***$p < 0.001$ (Student's *t*-test). Scale bars: 10 μm.

interacting 2) and LC3 were colocalized with Cy3-ISD (Fig. S4A). Moreover, knockout of *wipi2* but not *rb1cc1* abolished the colocalization between LC3 and Cy3-ISD (Fig. S4B). Given that WIPI2 is required for STING1-induced LC3 lipidation on autophagosomes but not single-membranes [34,35], these data imply that cytoplasmic DNA can be engulfed by autophagosomes. As autophagic substrates can be sequestered into autophagosomes [34,36,37], we further performed a DNase protection assay to test whether cytoplasmic DNA is indeed present in autophagosomes (Fig. S4C). Cells were transfected with Cy3-ISD and then subjected to mechanical disruption. After treating the samples with DNase, the fluorescence signal was still detectable in samples from WT or *rb1cc1* knockout cells, but it was undetectable in samples from *atg7* knockout cells (Fig. S4D). Moreover, reintroduction of WT ATG7 or ATG7-2KR but not ATG7-2KQ into *atg7* knockout cells restored the fluorescence signal (Fig. S4E). These results suggest that a portion of cytoplasmic DNA can be included within double-membrane autophagosomes and protected from DNase-mediated breakdown. We then checked the autophagic clearance of cytoplasmic DNA in cells. Consistent with previous observations [31,34], we found that cGAMP treatment stimulated the clearance of cytoplasmic Cy3-ISD in WT cells, but this effect was abolished in *atg7* knockout cells (Figure 4H,I). Moreover, reintroduction of WT ATG7 or ATG7-2KR, but not ATG7-2KQ, restored the capacity of cGAMP to stimulate the clearance of cytoplasmic Cy3-ISD (Figure 4H,I). As STING1-induced macroautophagy can promote the attenuation of CGAS-STING1 signaling by eliminating cytoplasmic DNA and STING1 [34,38], we further examined *Ifnb*1 (interferon beta 1) expression, an indicator of CGAS-STING1 signaling. Interestingly, ISD transfection stimulated higher *Ifnb1* expression in *atg7* knockout cells, and re-introduction of WT ATG7 or ATG7-2KR, but not ATG7-2KQ, attenuated ISD transfection-stimulated increase in the level of *Ifnb1* mRNA (Fig. S4F). These results suggest that deacetylation of ATG7 is required for STING1-induced macroautophagy and the clearance of cytoplasmic DNA, which in turn promotes the attenuation of CGAS-STING1 signaling.

Deacetylation of ATG7 is required for LC3-associated microautophagy

Accumulating evidence has shown that LC3 lipidation is also involved in the regulation of LC3-associated microautophagy [16,17]. Firstly, we treated the cells with ammonium chloride, monensin or nigericin, three inducers for LC3-associated microautophagy [16], and found that the acetylation level of ATG7 was significantly decreased (Figure 5A,B). Consistent with this, the interaction between ATG7 and ATG3 was increased in cells treated with ammonium chloride, monensin or nigericin (Fig. S5A,B). Moreover, the interaction between ATG3 and WT ATG7, but not ATG7-2KR or ATG7-2KQ, was promoted in monensin-treated cells (Fig. S5C,D). In addition, supporting the previous observation [16], we found that monensin treatment was able to induce LC3 lipidation on lysosomal membrane (Fig. S5E). Interestingly, knockout of *atg7* but not *rb1cc1* abolished GFP-LC3 punctum formation

in cells treated with monensin (Figure 5C,D). Re-introduction of WT ATG7 or ATG7-2KR, but not ATG7-2KQ, restored the formation of GFP-LC3 puncta in monensin-treated cells with *atg7* knockout (Figure 5C,D).
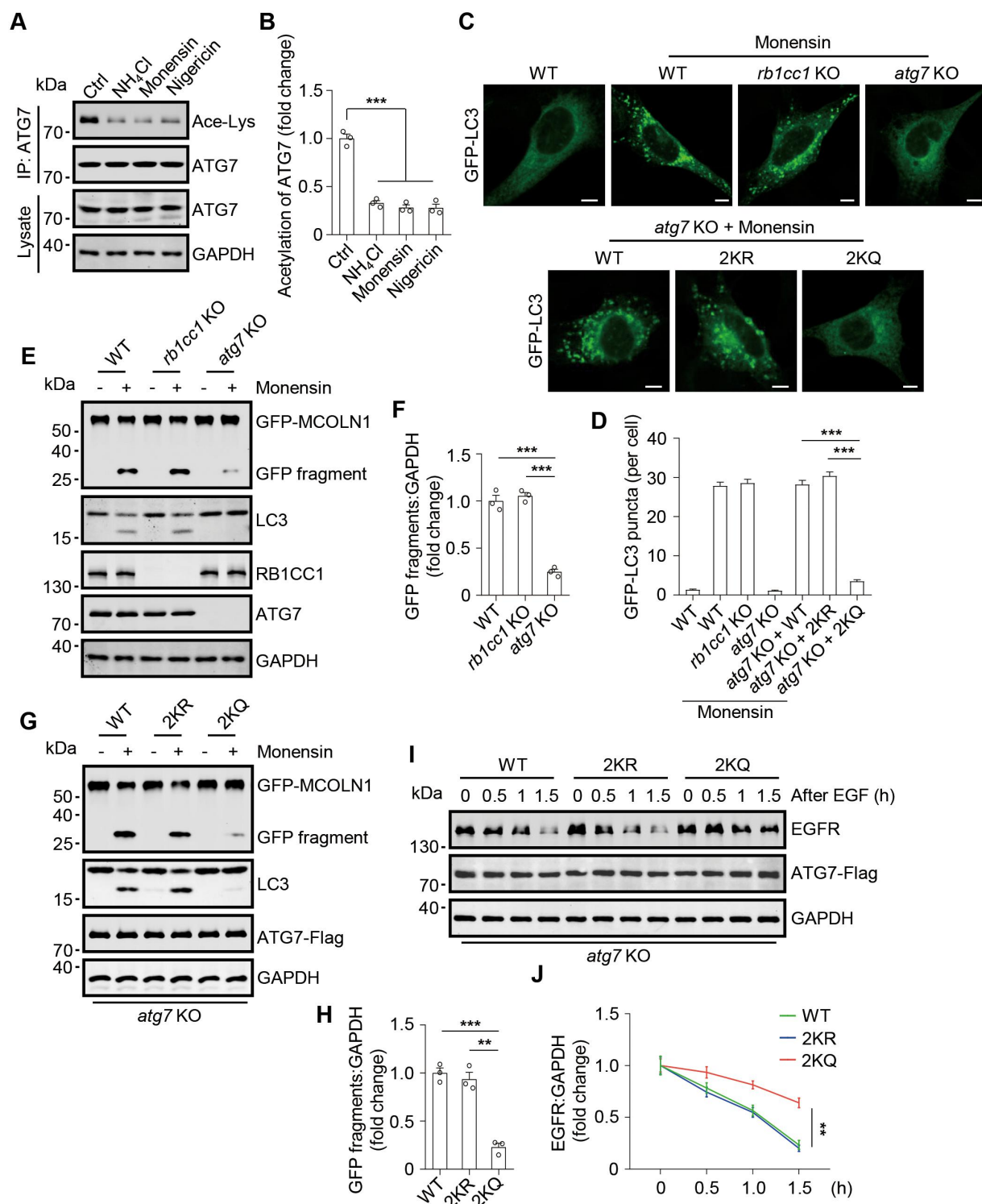
LC3-associated microautophagy is required for the selective turnover of lysosome membrane proteins, which is essential for the maintenance of lysosome activity under stress conditions [16]. We chose GFP-tagged MCOLN1/TRPML1 (mucolipin TRP cation channel 1), one of the substrates of LC3-associated microautophagy [16], as a reporter to indicate the selective turnover of lysosome membrane proteins. Obviously, monensin treatment led to the appearance of free GFP fragments from GFP-MCOLN1 in WT cells (Figure 5E, F). As expected, knockout of *atg7* but not *rb1cc1* significantly reduced GFP-MCOLN1 turnover (Figure 5E,F). Furthermore, in cells with *atg7* knockout, re-introduction of WT ATG7 or ATG7-2KR, but not ATG7-2KQ, restored monensin treatment-induced GFP-MCOLN1 turnover (Figure 5G,H). Finally, we checked lysosome activity by examining EGFR (epidermal growth factor receptor) degradation [39]. The *atg7* knockout cells with re-introduction of WT ATG7 or ATG7 mutants were subjected to 2-h monensin treatment and 4-h monensin washout, and then serum starved and stimulated with EGF. The protein level of EGFR decreased much faster in cells expressing WT ATG7 or ATG7-2KR than that in cells expressing ATG7-2KQ (Figure 5I,J).

Taken together, these data suggest that deacetylation of ATG7 is required for LC3-associated microautophagy, the selective turnover of lysosome membrane proteins, and the maintenance of lysosome activity under stress conditions.

Discussion

Protein acetylation has emerged as a master regulator of macroautophagy by targeting a great number of proteins, functioning in many distinct steps [1]. Among the identified proteins targeted by protein acetylation, several are core components involved in LC3 lipidation reaction [1]. In addition to macroautophagy, lipidated LC3 has been shown to regulate LC3-associated microautophagy [16,17]. Here, we unravel a previously unappreciated ATG7-based regulation mechanism for LC3 lipidation in the cell in response to various different stimuli. By promoting the interaction between ATG7 and ATG3, deacetylation of ATG7 markedly activates LC3 lipidation and drives the induction of maroautophagy or LC3-associated microautophagy under distinct stress conditions (Figure 6).

It is worth noting that, LC3 lipidation controls many different membrane events in the cell, such as LC3-assoicatd phagocytosis and macropinocytosis [40,41]. In addition to macroautophagy and LC3-associated microautophagy, acetylation of ATG7 may also be involved in the regulation of these LC3 lipidation-dependent cellular processes. Of note, many autophagy-related proteins, including ATG5 and ATG7, can regulate a number of autophagy- or LC3 lipidation-independent processes, such as gene transcription and DNA damage response [42–44]. Posttranslational modifications (PTMs) of these proteins may also regulate their function in some autophagy-independent

Figure 5. Deacetylation of ATG7 is required for LC3-associated microautophagy. (A) acetylation of ATG7 in MEFs treated with ammonium chloride, monensin or nigericin. (B) statistical analysis of (A). (C) formation of GFP-LC3 puncta in MEFs stably expressing GFP-LC3. The cells with or without *rb1cc1* or *atg7* knockout were re-introduced with or without WT ATG7, ATG7-2KR or ATG7-2KQ, and treated with or without monensin for 2 h. Scale bars: 10 μm. (D) statistical analysis of the number of GFP-LC3 puncta in cells treated as in (C). $n = 30$. (E) GFP-MCOLN1 turnover in MEFs. The cells with or without knockout of *rb1cc1* or *atg7* were treated with or without monensin for 8 h. GFP-tagged full-length MCOLN1 and free GFP fragments are indicated. (F) statistical analysis of the production of free GFP fragments in (E). (G) GFP-MCOLN1 turnover in *atg7* knockout MEFs with re-introduction of WT ATG7, ATG7-2KR or ATG7-2KQ. The cells were treated with or without monensin for 8 h. (H) statistical analysis of the production of free GFP fragments in (G). (I) EGFR degradation in *atg7* knockout MEFs with re-introduction of WT ATG7, ATG7-2KR or ATG7-2KQ. The cells were subjected to 2-h monensin treatment and 4-h monensin washout, and then serum starved and stimulated by EGF with the indicated times. (J) statistical analysis of (I). All statistical data are presented as mean ± SEM of three independent experiments. $**p < 0.01$, $***p < 0.001$ (Student's *t*-test).

processes. Thus, it would be interesting to explore whether acetylation regulates the function of ATG7 in some LC3 lipidation-independent cellular processes.

Protein acetylation is a reversible PTM, and the acetylation status of the targets is highly dynamic and coordinately controlled by the specific acetyltransferase and deacetylase. In this
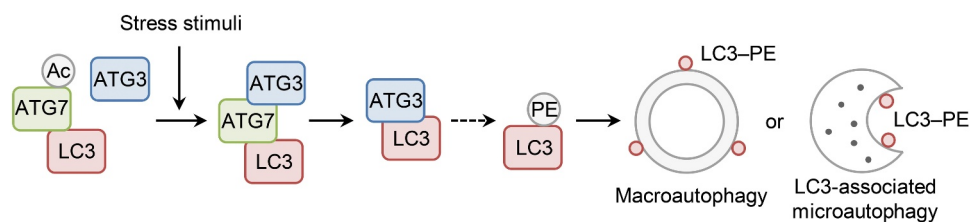
Figure 6. Schematic model for the role of ATG7 acetylation in the induction of macroautophagy and LC3-associated microautophagy. In response to various intracellular or environmental stimuli, ATG7 undergoes deacetylation, which promotes the interaction between ATG7 and ATG3, leading to the activation of LC3 lipidation and the induction of macroautophagy or LC3-associated microautophagy.

study, we have shown that the acetylation level of ATG7 is markedly decreased or increased in the cell upon different stimuli. Considering that the acetylation of ATG7 is determined by acetyltransferase EP300-CREBBP and deacetylase SIRT1 [21,22], it would need further investigation to clarify the role of EP300-CREBBP and SIRT1 in controlling the acetylation of ATG7 in the cell under different stress conditions. Of note, the activity of EP300-CREBBP and SIRT1 in the cell has been demonstrated to be tightly controlled by energy and nutrient sensors, including AMP-activated protein kinase (AMPK) and MTORC1 [45–48]. Therefore, it is highly possible that AMPK or MTORC1 may integrate distinct intracellular or environmental cues to control the induction of macroautophagy or LC3-associated microautophagy by regulating the activity of EP300-CREBBP or SIRT1.

In addition to LC3 and ATG7, the role of acetylation of ATG5 and ATG12, two core components involved in LC3 lipidation reaction, in macroautophagy, LC3-associated microautophagy and other LC3 lipidation-related processes remains unclear and needs further investigation. Notably, ATG5 has been reported to regulate DNA damage response through an autophagy-independent manner [43]. Moreover, EP300-CREBBP and SIRT1, determining the acetylation status of ATG5, play key roles in DNA damage response [48,49]. It is possible that EP300-CREBBP- and SIRT1-regulated acetylation of ATG5 may also controls its function in DNA damage response.

Materials and methods

Plasmids and oligonucleotides

EP300-Flag was a gift from Dr. Shimin Zhao (Fudan University, China) [25]. ATG7-Flag was constructed by inserting mouse cDNA of *Atg7* into a pcDNA3-Flag vector [46]. GST-tagged WT ATG7, ATG7-2KR, ATG7-2KQ, ATG3, WT LC3, LC3-2KQ and LC3-G120 (the processed form of LC3) were constructed by inserting the corresponding cDNA into a pGEX-4T-1 vector [46]. GFP-MCOLN1 was constructed by inserting the cDNA of MCOLN1 into a pEGFP-C1 vector (Clontech, PT3028–5). GFP-LC3 was described previously [50]. Site-directed mutagenesis was performed using QuikChange II XL (Agilent Technologies, 200516) according to the manufacturer's instructions. The following siRNA duplexes were used, human *EP300* siRNA, sense, CUAGAGACACCUUGUAGUAUU, anti-sense, UACUAC AAGGUGUCUCUAGUU; human *CREBBP* siRNA, sense, AAUCCACAGUACCGAGAAAUGUU, anti-sense, CAUUUCUCGGUACUGUGGAUUUU; human *SIRT1* siRNA,

sense, GAUGAAGUUGACCUCCUCAUU, anti-sense, UGAGGAGGUCAACUUCAUCUU; mouse *Atg7* siRNA, sense, GCUAGAGACGUGACACAUAUU, anti-sense; UAUGUGUCACGUCUCUAGCUU; Non-targeting siRNA, sense, UUCUCCGAACGUGUCACGUUU, anti-sense, ACGUGACACGUUCGGAGAAUU. The following Cy3-ISD sequences were used [51], sense, Cy3-TACAGATCTACTAGTGATCTATGACTGATCTGTACATG-ATCTACA, anti-sense, TGTAGATCATGTACAGATCAGTC ATAGATCACTAGTAGATCTGTA. For real-time PCR analysis, the following primers were used, mouse *Ifnb1* forward, AGGGCGGACTTCAAGATC, reverse, CTCATTCC ACCCAGTGCT; mouse *Actb* forward, GGCTGTATTCCCCTCCATCG, reverse, CCAGTTGGT AACAATGCCATGT.

Antibodies

The following primary antibodies were used, anti-WIPI2 (mouse; Abcam, ab105459), anti-acetyl-lysine (rabbit; Cell Signaling Technology, 9441), anti-CREBBP/CBP (rabbit; Cell Signaling Technology, 7389S), anti-LAMP1 (rabbit; Cell Signaling Technology, 9091S), anti-SIRT1 (mouse; Cell Signaling Technology, 8469S), anti-GST (rabbit; Huabio, ET1611–47), anti-Flag (mouse; MBL, M185-3 L), anti-Flag (rabbit; MBL, PM020), anti-LC3 (rabbit; MBL, PM036), anti-EGFR (rabbit; Proteintech, 18986–1-AP), anti-RB1CC1 /FIP200 (rabbit; Proteintech, 17250–1-AP), anti-GAPDH (rabbit; Proteintech, 10494–1-AP), anti-SQSTM1/p62 (rabbit; Proteintech, 18420–1-AP), anti-GFP (mouse; Santa Cruz Biotechnology, sc-9996), anti-ATG3 (rabbit; Sigma-Aldrich, A3606), anti-ATG7 (rabbit; Sigma-Aldrich, A2856), anti-EP300/p300 (mouse; Sigma-Aldrich, 05–257). The following secondary antibodies were used for western blot, donkey anti-rabbit IgG (H+L) IRDye800CW (LI-COR Biosciences, 926–32213), donkey anti-mouse IgG (H+L) IRDye680RD (LI-COR Biosciences, 926–68072). The following secondary antibodies were used for immunostaining, goat anti-mouse IgG (H+L), Alexa Fluor 488 (Thermo Fisher Scientific, A-11001), donkey anti-rabbit IgG (H+L), Alexa Fluor 488 (Thermo Fisher Scientific, A-21206), donkey anti-rabbit IgG (H+L), Alexa Fluor 546 (Thermo Fisher Scientific, A10040). Anti-Flag magnetic beads (Bimake, B26102) were used for immunoprecipitation assay, glutathione-sepharose 4B beads (GE Healthcare Life Sciences, 17-0756-01) were used for GST affinity-isolation assay.

Reagents and treatment

The chemicals were used as follows unless indicated otherwise: cGAMP (InvivoGen, tlrl-nacga23–1), 500 nM; torin1 (Selleck, S2827), 250 nM, 3 h; chloroquine, 10 μM, 3 h; trichostatin A (Selleck, S1054), 400 nM, 16 h; nicotinamide (Sigma-Aldrich, 72340), 5 mM, 8 h; CTB (Sigma-Aldrich, C6499), 50 μM, 6 h; C646 (Selleck, S7152), 10 μM), 4 h; EX-527 (Selleck, S1541), 25 μM, 6 h; monensin (Selleck, S2324), 50 μM; NH_4Cl (Sigma-Aldrich, 254134), 10 mM; nigericin (Selleck, S6653), 25 μM. cGAMP was delivered into cells by permeabilization with digitonin (10 μg/ml; Selleck, E1321) for 15 min in a buffer (50 mM HEPES-KOH, pH 7.2, 100 mM KCl, 3 mM $MgCl_2$, 0.1 mM DTT [Sangon Biotech, A620058], 85 mM sucrose [Sangon Biotech, A502792], 0.2% BSA [Sigma-Aldrich, A1933], 1 mM ATP [Selleck, S1985]). Cells were incubated with starvation medium (1% BSA, 140 mM NaCl, 1 mM $CaCl_2$, 1 mM $MgCl_2$, 5 mM glucose, and 20 mM HEPES, pH 7.4), referred to as starvation.

Cell culture and transfection

HEK293 and 293T cells and mouse embryonic fibroblasts (MEFs) were described previously [34,46,50], and cultured in Dulbecco Modified Eagle Medium (Gibco, 11965092) supplemented with 10% fetal bovine serum (Gibco, 10091148) in a 37°C incubator with a humidified, 5% CO_2 atmosphere. Lipofectamine 3000 (Invitrogen, L3000015) was used for the transfection of plasmids, siRNA duplexes and ISDs according to the manufacturer's instructions. To achieve the maximal RNAi efficacy, the transfection of siRNA duplexes was repeated twice with an interval of 24 h. HEK293 cells and MEFs stably expressing GFP-LC3 were generated as described previously [34,50]. MEFs stably expressing Flag-tagged, WT ATG7, ATG7-2KR and ATG7-2KQ were generated by transient transfection and selected with G418 (Sigma-Aldrich, A1720). MEFs with rb1cc1, atg5 or atg7 knockout were described previously [20,52].

Immunostaining and cell imaging

Cells were fixed in 4% formaldehyde for 10 min at room temperature. After washing twice with PBS (Sangon Biotech, E607008), cells were incubated in PBS containing 10% fetal calf serum (Sigma, F0685) to block nonspecific sites of antibody adsorption. The cells were then incubated with the appropriate primary antibodies and secondary antibodies in PBS containing 0.1% saponin (Sigma, S7900) and 10% fetal calf serum as indicated. After immunostaining, the cell nuclei were stained with DAPI Fluoromount-G (Southern Biotech, 0100–20). Confocal images were captured in multitracking mode on a Meta laser-scanning confocal microscope 880 (Carl Zeiss) with a 63× Plan Apochromat 1.4 NA objective and analyzed with the LSM 880 software.

Western blot and immunoprecipitation

Western blot was performed as described previously [53]. In brief, samples were separated with SDS-PAGE, transferred to polyvinylidene difluoride (PVDF) membrane and probed with the corresponding antibodies. The specific bands were analyzed using an Odyssey Infrared Imaging System. For immunoprecipitation, cells were lysed in Nonidet P40 (NP-40) buffer (50 mM Tris-HCl, pH 7.4, 1% NP-40 [Sangon Biotech, A100109], 150 mM NaCl, 2 mM EDTA, 1 mM DTT, 10% glycerol) supplemented with protease inhibitors (Roche, 4693159001) and phosphatase inhibitors (Sangon Biotech, C500017). The cell lysates were mixed with anti-Flag magnetic beads or the appropriate primary antibodies at 4°C overnight. For the latter, the cell lysates were further incubated with protein A or G sepharose beads for another 2 h. After that, the immunocomplexes were washed extensively 4 times and resolved in SDS sample buffer. The samples were subjected to western blot analysis.

Protein expression and purification

GST-tagged WT ATG7, ATG7-2KR, ATG7-2KQ, ATG3, WT LC3, LC3-2KQ and LC3-G120 (the processed form of LC3) were expressed in *Escherichia coli* BL21 (Transgen Biotech, CD601) by induction with 0.1 mM isopropyl β-D-thiogalactopyranoside (Sigma-Aldrich, I5502) for 12 h at 28°C. The recombinant proteins were purified using glutathione-sepharose 4B beads, and eluted with glutathione (Beyotime, S0073) or incubated with thrombin protease (Sigma-Aldrich, T4648) at 4°C for 6 h to release the proteins from the GST.

In vitro GST affinity-isolation assay

Purified GST, GST-tagged WT ATG7, ATG7-2KR, ATG7-2KQ, WT LC3 or LC3-2KQ proteins were incubated with purified ATG3, WT ATG7, ATG7-2KR or ATG7-2KQ proteins. After incubation for 4 h at 4°C, glutathione-sepharose 4B beads were added to the mixture, followed by further incubation for 2 h at 4°C. The beads were washed with NP-40 buffer 4 times. The beads-bound proteins were subjected to western blot analysis.

In vitro acetylation assay

The *in vitro* acetylation assay was performed as described previously [46,54]. Briefly, the reaction was performed in 30 μl of reaction buffer (20 mM Tris-HCl, pH 8.0, 20% glycerol, 100 mM KCl, 1 mM DTT and 0.2 mM EDTA) in the presence of 20 μM acetyl-CoA (Sigma-Aldrich, 10101893001). Immunoprecipitated EP300-Flag from 293T cells and recombinant GST-tagged WT ATG7 or ATG7-2KR from *Escherichia coli* BL21 cells were added. After incubation at 30°C for 1 h, the reaction was terminated by the addition of 10 μl of SDS sample buffer. The samples were subjected to western blot analysis.

In vitro LC3 lipidation assay

The *in vitro* LC3 assay was described previously with some modifications [26]. The cytosol was prepared from MEFs with atg7 knockout grown in normal culture medium. After

washing with PBS, cells were lysed by passing through a 25 G needle in a 3×cell pellet volume of hypotonic buffer (20 mM HEPES-KOH, pH 7.2, 10 mM KCl, 3 mM MgCl$_2$) plus a cocktail of protease inhibitors (Roche, 4693159001) and phosphatase inhibitors (Sangon Biotech, C500017). The cell lysate was centrifuged at 100,000 g for 2 h to collect the supernatant. For membrane preparation, MEFs with *atg5* knockout grown in normal culture medium, were washed with PBS (Sangon Biotech, E607008) and homogenized by douncing for 20 times in a buffer (20 mM HEPES-KOH, 400 mM sucrose, 0.5 mM EDTA). The homogenate was centrifuged at 1,000 g for 5 min to remove cell debris and nuclei. The supernatant was further centrifuged at 5,000 g for 10 min to precipitate mitochondria and other heavy organelles. The supernatant was further centrifuged at 25,000 g for 30 min to pellet membranes. For each reaction, the cytosol, the membranes, purified Flag-tagged WT ATG7, ATG7-2KR or ATG7-2KQ, GST-LC3-G120 (the processed form of LC3) and ATP regeneration system (40 mM creatine phosphate [Sangon Biotech, A610821], 0.2 mg/ml creatine phosphokinase [Sangon Biotech, A600327], and 1 mM ATP), and GTP (0.15 mM; Sangon Biotech, A620332) were incubated in a final volume of 30 μl. The mixture was incubated at 30°C for the indicated time, and the reaction was terminated by the addition of 10 μl of SDS sample buffer. The samples were subjected to western blot analysis.

EGFR degradation assay

The *atg7* knockout cells with re-introduction of WT ATG7, ATG7-2KR or ATG7-2KQ were subjected to 2-h monensin treatment and 4-h monensin washout, and then cultured in serum-free DMEM for 12 h, followed by incubation on ice in serum-free DMEM containing 100 ng/ml of EGF (Beyotime, P6114) for 15 min. The cells were washed with PBS to remove excess EGF followed by culturing in serum-free DMEM at 37°C for the indicated time. Then the cells were lysed and subjected to western blot analysis.

DNase protection assay

Cells transfected with Cy3-ISD were harvested, washed, and homogenized in extraction buffer (5 mM MOPS [Sangon Biotech, A620360], pH 7.65, 0.25 M sucrose, 1 mM EDTA, 0.1% ethanol). The samples were pelleted at 150 g for 5 min at 4°C to pellet debris. The resulting samples were incubated with DNase (Beyotime, D7076) and/or 0.5% Triton X-100 (Sangon Biotech, A600198) for 90 min at 37°C, and then the fluorescence intensity was assessed by measuring the fluorescent emission at 569 nm following excitation at 555 nm.

RNA extraction and real-time PCR

Total RNA was isolated from cells by TRIzol reagent (Thermo Fisher Scientific, 15596018) and was reverse transcribed into cDNA using M-MLV reverse transcription reagents

(Promega, A5000). The resulting cDNA was subjected to real-time PCR analysis with gene-specific primers.

HPLC-MS/Ms

To identify the acetylation site(s) of ATG7 by mass spectrometry, the gel band of acetylated GST-ATG7 was excised. In-gel digestion of GST-ATG7 was performed with MS-grade modified trypsin (Promega, V5111) at 37°C overnight. The digested peptides were desalted and loaded on a capillary reverse-phase C18 column packed in-house (15-cm in length, 100 μm ID × 360 μm OD, 3-μm particle size, 100-Å pore diameter) connected to an Easy LC 1000 system (Thermo Fisher Scientific). The samples were analyzed with a 180-min HPLC gradient from 0% to 100% buffer B (buffer A: 0.1% formic acid in water; buffer B: 0.1% formic acid in acetonitrile) at 300 nL/min. The eluted peptides were ionized and directly introduced into a Q-Exactive or Fusion mass spectrometer (Thermo Fisher Scientific) using a nano-spray source. Survey full-scan MS spectra (m/z 300–1800) were acquired in the Orbitrap analyzer with resolution $r = 70,000$ at m/z 400.

Statistical analysis

All the statistical data are presented as mean ± SEM. The statistical significance of differences was determined using Student's *t*-test. $p < 0.05$ was considered to be statistically significant.

References

[1] Xu Y, Wan W. Acetylation in the regulation of autophagy. Autophagy. 2023;19(2):379–387. doi: 10.1080/15548627.2022.2062112

[2] Yim WW, Mizushima N. Lysosome biology in autophagy. Cell Discov. 2020;6:6. doi: 10.1038/s41421-020-0141-7

[3] Xu Y, Wan W. Emerging roles of p300/CBP in autophagy and autophagy-related human disorders. J Cell Sci. 2023;136(12): jcs261028. doi: 10.1242/jcs.261028

[4] Yamamoto H, Matsui T. Molecular mechanisms of macroauto-phagy, microautophagy, and chaperone-mediated autophagy. J Nippon Med Sch. 2023. doi: 10.1272/jnms.JNMS.2024_91-102

[5] Feng Y, He D, Yao Z, et al. The machinery of macroautophagy. Cell Res. 2014;24(1):24–41. doi: 10.1038/cr.2013.168

[6] Wang L, Klionsky DJ, Shen HM. The emerging mechanisms and functions of microautophagy. Nat Rev Mol Cell Biol. 2022;24:186–203. doi: 10.1038/s41580-022-00529-z

[7] Kaushik S, Cuervo AM. The coming of age of chaperone-mediated autophagy. Nat Rev Mol Cell Biol. 2018;19 (6):365–381. doi: 10.1038/s41580-018-0001-6

[8] Klionsky DJ, Petroni G, Amaravadi RK, et al. Autophagy in major human diseases. EMBO J. 2021;40:e108863. doi: 10.15252/embj.2021108863

[9] Mizushima N, Levine B, Longo DL. Autophagy in human diseases. N Engl J Med. 2020;383(16):1564–1576. doi: 10.1056/NEJMra2022774

[10] Yamamoto H, Zhang S, Mizushima N. Autophagy genes in biol-ogy and disease. Nat Rev Genet. 2023;24(6):382–400. doi: 10.1038/s41576-022-00562-w

[11] Joachim J, Tooze SA. GABARAP activates ULK1 and traffics from the centrosome dependent on Golgi partners WAC and GOLGA2/GM130. Autophagy. 2016;12(5):892–893. doi: 10.1080/15548627.2016.1159368

[12] Kumar S, Jain A, Farzam F, et al. Mechanism of Stx17 recruitment to autophagosomes via IRGM and mammalian Atg8 proteins. J Cell Bio. 2018;217(3):997–1013. doi: 10.1083/jcb.201708039

[13] Nakatogawa H, Ichimura Y, Ohsumi Y. Atg8, a ubiquitin-like protein required for autophagosome formation, mediates mem-brane tethering and hemifusion. Cell. 2007;130(1):165–178. doi: 10.1016/j.cell.2007.05.021

[14] Nguyen TN, Padman BS, Usher J, et al. Atg8 family LC3/GABARAP proteins are crucial for autophagosome-lysosome fusion but not autophagosome formation during PINK1/Parkin mitophagy and starvation. J Cell Bio. 2016;215:857–874. doi: 10.1083/jcb.201607039

[15] Pankiv S, Clausen TH, Lamark T, et al. p62/SQSTM1 binds directly to Atg8/LC3 to facilitate degradation of ubiquitinated protein aggregates by autophagy. J Biol Chem. 2007;282 (33):24131–24145. doi: 10.1074/jbc.M702824200

[16] Lee C, Lamech L, Johns E, et al. Selective lysosome membrane turnover is induced by nutrient starvation. Dev Cell. 2020;55:289–297. doi: 10.1016/j.devcel.2020.08.008

[17] Mejlvang J, Olsvik H, Svenning S, et al. Starvation induces rapid degradation of selective autophagy receptors by endosomal microautophagy. J Cell Bio. 2018;217(10):3640–3655. doi: 10.1083/jcb.201711002

[18] Mizushima N. The ATG conjugation systems in autophagy. Curr Opin Cell Biol. 2020;63:1–10. doi: 10.1016/j.ceb.2019.12.001

[19] Yi C, Ma M, Ran L, et al. Function and molecular mechanism of acetylation in autophagy regulation. Science. 2012;336 (6080):474–477. doi: 10.1126/science.1216990

[20] Huang R, Xu Y, Wan W, et al. Deacetylation of nuclear LC3 drives autophagy initiation under starvation. Mol Cell. 2015;57 (3):456–466. doi: 10.1016/j.molcel.2014.12.013

[21] Lee IH, Cao L, Mostoslavsky R, et al. A role for the NAD-dependent deacetylase Sirt1 in the regulation of autophagy. Proc Natl Acad Sci U S A. 2008;105(9):3374–3379. doi: 10.1073/pnas.0712145105

[22] Lee IH, Finkel T. Regulation of autophagy by the p300 acetyltransferase. J Biol Chem. 2009;284(10):6322–6328. doi: 10.1074/jbc.M807135200

[23] Sun L, Xiong H, Chen L, et al. Deacetylation of ATG4B promotes autophagy initiation under starvation. Sci Adv. 2022;8(31):eabo0412. doi: 10.1126/sciadv.abo0412

[24] Fletcher K, Ulferts R, Jacquin E, et al. The WD40 domain of ATG16L1 is required for its non-canonical role in lipidation of LC3 at single membranes. EMBO J. 2018;37(4):e97840. doi: 10.15252/embj.201797840

[25] Jiang W, Wang S, Xiao M, et al. Acetylation regulates gluconeo-genesis by promoting PEPCK1 degradation via recruiting the UBR5 ubiquitin ligase. Mol Cell. 2011;43(1):33–44. doi: 10.1016/j.molcel.2011.04.028

[26] Ge L, Melville D, Zhang M, et al. The ER-Golgi intermediate compartment is a key membrane source for the LC3 lipidation step of autophagosome biogenesis. Elife. 2013;2:e00947. doi: 10.7554/eLife.00947

[27] Fujita N, Itoh T, Omori H, et al. The Atg16L complex specifies the site of LC3 lipidation for membrane biogenesis in autophagy. Mol Biol Cell. 2008;19(5):2092–2100. doi: 10.1091/mbc.e07-12-1257

[28] Hong SB, Kim BW, Lee KE, et al. Insights into noncanonical E1 enzyme activation from the structure of autophagic E1 Atg7 with Atg8. Nat Struct Mol Biol. 2011;18(12):1323–1330. doi: 10.1038/nsmb.2165

[29] Noda NN, Satoo K, Fujioka Y, et al. Structural basis of Atg8 activation by a homodimeric E1, Atg7. Mol Cell. 2011;44 (3):462–475. doi: 10.1016/j.molcel.2011.08.035

[30] Taherbhoy AM, Tait SW, Kaiser SE, et al. Atg8 transfer from Atg7 to Atg3: a distinctive E1-E2 architecture and mechanism in the autophagy pathway. Mol Cell. 2011;44(3):451–461. doi: 10.1016/j.molcel.2011.08.034

[31] Gui X, Yang H, Li T, et al. Autophagy induction via STING trafficking is a primordial function of the cGAS pathway. Nature. 2019;567(7747):262–266. doi: 10.1038/s41586-019-1006-9

[32] Liu D, Wu H, Wang C, et al. STING directly activates autophagy to tune the innate immune response. Cell Death Differ. 2019;26 (9):1735–1749. doi: 10.1038/s41418-018-0251-z

[33] Wan W, Liu W. STING recruits WIPI2 for autophagosome formation. Autophagy. 2023. doi: 10.1080/15548627.2023.2202108

[34] Wan W, Qian C, Wang Q, et al. STING directly recruits WIPI2 for autophagosome formation during STING-induced autophagy. EMBO J. 2023;42(8):e112387. doi: 10.15252/embj.2022112387

[35] Fischer TD, Wang C, Padman BS, et al. STING induces LC3B lipidation onto single-membrane vesicles via the V-ATPase and ATG16L1-WD40 domain. J Cell Bio. 2020;219(12):e202009128. doi: 10.1083/jcb.202009128

[36] Ohnstad AE, Delgado JM, North BJ, et al. Receptor-mediated clustering of FIP200 bypasses the role of LC3 lipidation in autophagy. EMBO J. 2020;39(24):e104948. doi: 10.15252/embj.2020104948

[37] Valverde DP, Yu SL, Boggavarapu V, et al. ATG2 transports lipids to promote autophagosome biogenesis. J Cell Bio. 2019;218 (6):1787–1798. doi: 10.1083/jcb.201811139

[38] Prabakaran T, Bodda C, Krapp C, et al. Attenuation of cGAS-STING signaling is mediated by a p62/SQSTM1-dependent autophagy pathway activated by TBK1. EMBO J. 2018;37(8):e97858. doi: 10.15252/embj.201797858

[39] Xu YF, Wan W. TP53INP2 mediates autophagic degradation of ubiquitinated proteins through its ubiquitin-interacting motif. FEBS Lett. 2019;593(15):1974–1982. doi: 10.1002/1873-3468.13467

[40] Heckmann BL, Green DR. LC3-associated phagocytosis at a glance. J Cell Sci. 2019;132(5):jcs222984. doi: 10.1242/jcs.222984

[41] Pena-Martinez C, Rickman AD, Heckmann BL. Beyond autopha-gy: LC3-associated phagocytosis and endocytosis. Sci Adv. 2022;8:eabn1702. doi: 10.1126/sciadv.abn1702

[42] Lee IH, Kawai Y, Fergusson MM, et al. Atg7 modulates p53 activity to regulate cell cycle and survival during metabolic stress. Science. 2012;336:225–228.

[43] Maskey D, Yousefi S, Schmid I, et al. ATG5 is induced by DNA-damaging agents and promotes mitotic catastrophe inde-pendent of autophagy. Nat Commun. 2013;4(1):2130. doi: 10.1038/ncomms3130

[44] Xu Y, Wan W, Shou X, et al. TP53INP2/DOR, a mediator of cell autophagy, promotes rDNA transcription via facilitating the assembly of the POLR1/RNA polymerase I preinitiation complex at rDNA promoters. Autophagy. 2016;12(7):1118–1128. doi: 10.1080/15548627.2016.1175693

[45] Chang CM, Su H, Zhang DH, et al. AMPK-dependent phosphorylation of GAPDH triggers Sirt1 activation and is necessary for autophagy upon glucose starvation. Mol Cell. 2015;60(6):930–940. doi: 10.1016/j.molcel.2015.10.037

[46] Wan W, You Z, Xu Y, et al. mTORC1 phosphorylates acetyltransferase p300 to regulate autophagy and lipogenesis. Mol Cell. 2017;68:323–335. doi: 10.1016/j.molcel.2017.09.020

[47] Yang WB, Hong YH, Shen XQ, et al. Regulation of transcription by AMP-activated protein kinase: phosphorylation of p300 blocks its interaction with nuclear receptors. J Biol Chem. 2001;276 (42):38341–38344. doi: 10.1074/jbc.C100316200

[48] Alves-Fernandes DK, Jasiulionis MG. The role of SIRT1 on DNA damage response and epigenetic alterations in cancer. Int J Mol Sci. 2019;20(13):3153. doi: 10.3390/ijms20133153

[49] Dutto I, Scalera C, Prosperi E. CREBBP and p300 lysine acetyl transferases in the DNA damage response. Cell Mol Life Sci. 2018;75(8):1325–1338. doi: 10.1007/s00018-017-2717-4

[50] Wan W, You Z, Zhou L, et al. mTORC1-regulated and HUWE1-mediated WIPI2 degradation controls autophagy flux. Mol Cell. 2018;72:303–315. doi: 10.1016/j.molcel.2018.09.017

[51] Du MJ, Chen ZJJ. DNA-induced liquid phase condensation of cGAS activates innate immune signaling. Science. 2018;361 (6403):704–709. doi: 10.1126/science.aat1022

[52] Su H, Yang F, Wang Q, et al. VPS34 acetylation controls its lipid kinase activity and the initiation of canonical and non-canonical autophagy. Mol Cell. 2017;67:907–921. doi: 10.1016/j.molcel.2017.07.024

[53] Xu Y, Wu Y, Wang L, et al. Autophagy deficiency activates rDNA transcription. Autophagy. 2022;18(6):1338–1349. doi: 10.1080/15548627.2021.1974178

[54] Sen N, Hara MR, Kornberg MD, et al. Nitric oxide-induced nuclear GAPDH activates p300/CBP and mediates apoptosis. Nat Cell Biol. 2008;10(7):866–873. doi: 10.1038/ncb1747